the ionization threshold will be captured as they fly through the SNR, until near complete photoionization is achieved. The required number of photons for the complete photoionization of iron can be estimated, from the above parameters, as $\approx 5 \times 10^{56} m_1$, taking into account Auger ionization (*4*) and including the exceptional iron abundance detected here, 75 times higher than the solar value. On the other hand, during the first 13 s (duration of the time intervals A+B), this burst emits a time-averaged photon spectrum $dn = 4.2dE/E$ photons cm^{-2} s^{-1} in the observer's frame. Within this time interval, and for a standard cosmology, this corresponds to a total of 3.6×10^{57} ionizing photons, where every photon above the threshold has been weighted with the ratio of its cross section to that at the threshold. Furthermore, the density due to a $10 m_1 M_\odot$ star dispersed in a volume of radius D is about 10^5 cm^{-3}, implying long recombination time scales ($>10^5$ s), depending on the exact, but rapidly varying, temperature. Thus, we conclude that the burst has about the right number of photons to cause the complete photoionization of iron within the B time interval, with recombination providing no real countereffect. A similar conclusion, with a more elaborate computation, has been reached, for generic parameters, by Böttcher *et al.* (*4*).

The implication of the above discussion is that the iron-rich material is, most likely, located around the burst site and cannot be located by chance along the line of sight. In fact, from the column density and iron abundance derived from the B spectrum, we have found that the absorbing material has an iron content ~75 times that of the solar value, and we have deduced that only a SNR can be responsible for this absorption. Calling R_{SNR} the radius of the SNR, and D its distance from the burst site, if the SNR were really located by chance along the line of sight, it would intercept only a fraction $\delta\Omega \sim (R_{SNR}/D)^2$ of all bursts photons. For a chance alignment, $R_{SNR} \ll D$, so that $\delta\Omega \ll 1$; however, this reduced number of burst photons would still have to ionize the whole SNR, i.e., several solar masses of matter. Because we have determined above that this is just about feasible for $D \approx 10^{17}$ cm, it follows that this cannot be accomplished for a chance alignment, where of course $D \ll 10^{17}$ cm, and we should be able to see the absorption edge through the entire burst duration. Given that this is not the case, we deduce that the SNR cannot be located by chance along the line of sight.

Lastly, the nondetection of an iron line (3σ upper limit of 1.5 photons cm^{-2} s^{-1}) from the SNR is consistent with our model. Indeed, at least three factors may contribute to making the iron line weak. First, the burst may be beamed, whereas the line reemission certainly is not. Second, although we see the whole SNR, yet line reemission is diluted with respect to the burst duration T_B by the light transit time D/c in the ratio cT_B/D. Third, although fluorescence may be fast, recombination must be slow, owing to the low overall material densities on the order of 10^5 atoms/cm^3. Still, such a line should be present at later times, when the afterglow decreases sufficiently; four cases of this kind have been reported [GRB970508 (*18*), GRB970828 (*19*), GRB991216 (*20*), GRB000214 (*21*)].

Our results favor models in which GRBs originate from the collapse of very massive stars and are preceded by a supernova-like explosion.

References and Notes

1. B. Paczynski, *Astrophys. J.* **494**, L45 (1998).
2. M. Vietri, L. Stella, *Astrophys. J.* **507**, L45 (1998).
3. C. Weth, P. Meszaros, T. Kallman, M. Rees, *Astrophys. J.* **534**, 581 (2000).
4. M. Böttcher, D. D. Dermer, W. Crider, E. P. Liang, *Astron. Astrophys.* **343**, 111 (1999).
5. F. Frontera *et al.*, *Astron. Astrophys. Suppl. Ser.* **122**, 357 (1997).
6. E. Costa *et al.*, *Adv. Space Res.* **22/7**, 1129 (1998).
7. R. Jager *et al.*, *Astron. Astrophys. Suppl. Ser.* **125**, 557 (1997).
8. F. Frontera *et al.*, *Astrophys. J. Suppl. Ser.* **127**, 59 (2000).
9. N. Masetti *et al.*, *Astron. Astrophys.* **354**, 473 (2000).
10. S. Holland *et al.*, *GCN Circ. 753* (2000).
11. J. G. Cohen *et al.*, *Astrophys. J.* **538**, 29 (2000).
12. G. Boella *et al.*, *Astron. Astrophys. Suppl. Ser.* **122**, 299 (1997).
13. D. Band *et al.*, *Astrophys. J.* **413**, 281 (1993).
14. R. Morrison, D. McCammon, *Astrophys. J.* **270**, 119. (1983).
15. E. Anders, N. Gredesse, *Geochim. Cosmochim. Acta*, **53**, 197 (1989).
16. H. Tsunemi, E. Miyata, B. Aschenbach, J. Hiraga, D. Akutsu, *Publ. Astron. Soc. Jpn.*, in press.
17. S. E. Woosley and T. A. Weaver, *Annu. Rev. Astron. Astrophys.* **24**, 205 (1986).
18. L. Piro *et al.*, *Astrophys. J.* **514**, L77 (1999).
19. A. Yoshida *et al.*, *Astron. Astrophys. Suppl. Ser.* **138**, 433 (1999).
20. L. Piro *et al.*, *Science* **290**, 955 (2000).
21. L. A. Antonelli *et al.*, *Astrophys. J.*, in press.
22. L. Amati *et al.*, *Astron. Astrophys. Suppl. Ser.* **138**, 403 (1999).

23. Supported by the Italian Space Agency (ASI) and Italian National Research Council (CNR). BeppoSAX is a joint program of ASI and the Netherlands Agency for Aerospace Programs.

5 September 2000; accepted 10 October 2000

Observation of X-ray Lines from a Gamma-Ray Burst (GRB991216): Evidence of Moving Ejecta from the Progenitor

L. Piro,[1]* G. Garmire,[2] M. Garcia,[3] G. Stratta,[1] E. Costa,[1] M. Feroci,[1] P. Mészáros,[2] M. Vietri,[4] H. Bradt,[5] D. Frail,[6] F. Frontera,[7] J. Halpern,[8] J. Heise,[9] K. Hurley,[10] N. Kawai,[11] R. M. Kippen,[12] F. Marshall,[13] T. Murakami,[14] V. V. Sokolov,[15] T. Takeshima,[16] A. Yoshida[11]

We report on the discovery of two emission features observed in the x-ray spectrum of the afterglow of the gamma-ray burst (GRB) of 16 December 1999 by the Chandra X-ray Observatory. These features are identified with the Ly_α line and the narrow recombination continuum by hydrogenic ions of iron at a redshift $z = 1.00 \pm 0.02$, providing an unambiguous measurement of the distance of a GRB. Line width and intensity imply that the progenitor of the GRB was a massive star system that ejected, before the GRB event, a quantity of iron ~0.01 of the mass of the sun at a velocity ~0.1 of the speed of light, probably by a supernova explosion.

The nature of the progenitors of GRBs is an unsettled issue of extreme importance (*1*). The merging of a binary system of compact objects (such as black holes, neutron stars, and white dwarfs) or the collapse of a massive star (hypernova or collapsar) could deliver the energy required by a GRB, but observational evidence favoring a particular model is still missing. This evidence can be gathered through the measurement of lines produced by the medium surrounding the GRB (*2–4*). However, although observations of GRB afterglows have provided much information on the broadband spectral continuum and its origin (*5, 6*), they have not yet given results of comparable importance on spectral lines. In the optical range, current measurements are inconclusive, because all of the spectral emission lines observed so far are produced by the host galaxy rather than at the burst site. The x-ray range appears more promising because theoretical computations show that only a dense, massive medium close to the GRB site—such as that expected in the case of a massive progenitor—could produce an iron emission line detectable with current x-ray instrumentation (*7–10*). Indeed, marginal evidence of iron features has been claimed in two x-ray afterglows (*11, 12*), but the case is still controversial because of the limited statistical weight as well as the tight upper limits measured in other afterglows (*13*), and because the claimed inconsistency between the redshift derived for GB970828 in x-rays and from the host galaxy (*14*) could be reconciled only by assuming different physical conditions in the two bursts (*9*). The prospect of gathering unique data on the nature of the progenitor made the search for spectral features one of the primary objectives of a Chandra (*15*) GRB observation program.

The first Chandra observation of a GRB was performed on the event of 16 December 1999, one of the brightest GRBs ever detected by the Burst and Transient Source Experiment (BATSE) on board the Compton Gamma-Ray Observatory, with fluence $S_\gamma > 2.5 \times 10^{-4}$ erg cm^{-2} above 20 keV (*16*). Following the localization of a strong x-ray afterglow by Rossi X-ray Transient Explorer (XTE; guided by the rapid BATSE GRB localization) and the characterization of its temporal behavior (*17*), and a confirming localization by the interplanetary network (*18*), we estimated that the x-ray flux would only decay to $\sim 10^{-12}$ erg cm^{-2} s^{-1} by the time Chandra could be reoriented to point at it. This flux level is high enough to use the gratings in conjunction with the Advanced CCD Imaging Spectrometer in the Spectroscopic configuration (ACIS-S), and we selected this instrument configuration for the observation. Chandra acquired the target on 18 December, 04:38 universal time (i.e., 37 hours after the GRB) and observed it for 3.4 hours. We found a bright x-ray source (*19*) with a position [right ascension (2000) = $05^h09^m31^s.35$, declination (2000) = $11°17'05''.7$] coincident within the 1.5″ error with the optical (*20*) and radio (*21*) transients and with a flux consistent with that expected from the XTE extrapolation.

The spectrum of the x-ray afterglow (Fig. 1) shows an emission line at energy E = 3.49 ± 0.06 keV. Because of the ubiquity and prominence of iron lines in astrophysical objects (*22*), we argue that this line is associated with emission from iron. Some ambiguity remains in the rest energy of the emission. Iron K_α lines have rest energies ranging from 6.4 keV (fluorescence of neutral atoms) to 6.7 keV (He-like ions) or 6.97 keV (H-like ions). In those three cases we would obtain redshifts of z = 0.83 ± 0.02, z = 0.92 ± 0.02, and z = 1.00 ± 0.02, respectively. In particular, at higher energies the ACIS-S spectrum shows evidence of a recombination edge in emission at E = 4.4 ± 0.5 keV (Fig. 2). Identifying this feature with the iron recombination edge with rest energy of 9.28 keV gives z = 1.11 ± 0.11, consistent with the highest of the redshifts implied by the emission line.

An iron recombination edge at 9.28 keV is indeed expected when the iron emission is driven by photoionization and the medium is heavily ionized by the radiation produced by the GRB and its afterglow (*2, 9, 23*). If the medium lies in the line of sight, the edge is expected to be seen in absorption at early times (*3, 9*), and evidence of such a feature has been found in another GRB (*24*). At later times, when the medium becomes heavily ionized and recombination takes place, the edge is seen in emission. This is our case. In this condition, x-ray lines are produced almost exclusively through recombination of electrons on H-like iron (*25*). The measured intensities of the two features are also consistent with theoretical expectations [$I_{edge}/I_L \approx 0.93(k_B T)^{0.2}$ (*23*), where I_{edge} and I_L are the intensities of the recombination edge and emission lines, respectively; k_B is the Boltzmann constant, T is the electron temperature of the gas, and their product is expressed in keV]. We therefore conclude that the redshift of the GRB is z = 1.00 ± 0.02. We stress that this measurement is consistent with the most distant absorption system (z = 1.02) found in the line of sight toward GRB991216 by op-

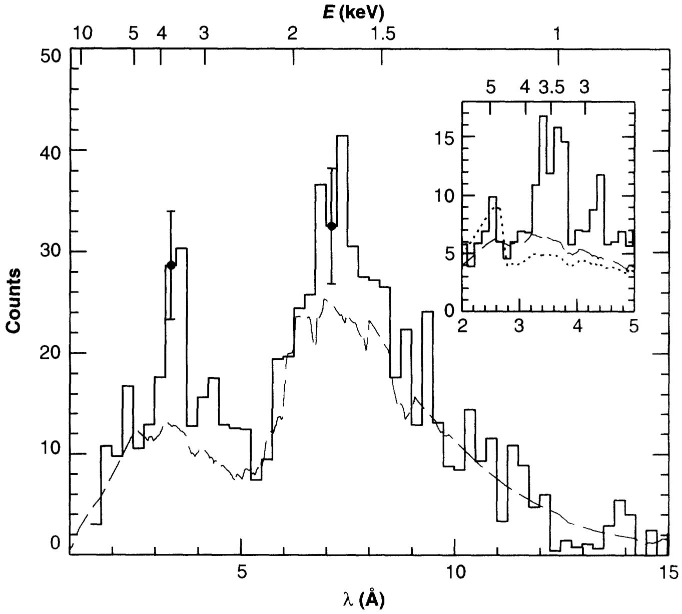

Fig. 1. The x-ray afterglow spectrum of GRB991216 obtained with the Chandra high-energy gratings [High Energy (HE) and Medium Energy (ME)] summed together. The background is negligible. The exposure time of the observation was 9700 s. For improved statistics, the grating spectrum has a bin size of 0.25 Å, including about 10 resolution elements of the ME and 20 of the HE. The dashed line represents the best-fit power law on the 0th order ACIS-S spectrum. The peak (i.e., 2 bins) around 3.5 Å (E = 3.5 keV) is detected with 4.7σ confidence. The error bars give the statistical Poissonian error of data points at 3.5 and 7 Å. We have verified the robustness of the detection against the continuum level. The significance remains above 4σ even when assuming a worst-case systematic uncertainty in the cross-calibration of the two instruments of 15% (*35*). In the inset, the region on the line is shown with a finer binning. The dotted line represents the best-fit continuum model to the 0th order ACIS-S spectrum after the addition of a recombination edge in emission (see Fig. 2). The line parameters (errors on best-fit parameters correspond to 90% confidence level for one parameter of interest) are I_L = 3.2 (±0.8) × 10^{-5} photons cm^{-2} s^{-1}, equivalent width = 0.5 ± 0.013 keV, width (σ_L) = 0.23 ± 0.07 keV, and E = 3.49 ± 0.06 keV. The spectrum has been examined at higher resolution to confirm the line broadening. Because each of the spectral bins in the figure includes several resolution elements of the instrument, a narrow feature would appear in no more than a single bin, regardless of how fine the binning is, but this is not the case. Deviations around 7 Å are ~3σ, and it is noteworthy that they are close to the expected energy (at z = 1.0) of the recombination edge of hydrogen-like sulfur. Deviations at ~4.4 Å are less than 3σ.

[1]Istituto Astrofisica Spaziale, Consiglio Nazionale delle Ricerche (CNR), Via Fosso del Cavaliere, 00133 Roma, Italy. [2]Department of Astronomy and Astrophysics, 525 Davey Lab, Pennsylvania State University, University Park, PA 16802, USA. [3]Harvard–Smithsonian Center for Astrophysics, 60 Garden Street, Cambridge, MA 02138, USA. [4]Department of Physics, Universita' Roma Tre, Via della Vasca Navale 84, 00146 Roma, Italy. [5]Massachusetts Institute of Technology, 77 Massachusetts Avenue, Cambridge, MA 02139, USA. [6]National Radio Astronomy Observatory, 1003 Lopezville Road, Socorro, NM 87801, USA. [7]Istituto Tecnologie e Studio Radiazioni Extraterrestri/CNR, Via Gobetti 101, 40129 Bologna, Italy. [8]Department of Astrophysics, Columbia University, New York, NY 10027, USA. [9]Space Research Organization in the Netherlands, Sorbonnelaan 2, 3584 CA Utrecht, Netherlands. [10]University of California Space Science Laboratory, Berkeley, CA 94720, USA. [11]Institute of Physical and Chemical Research (RIKEN), 2-1 Hirosawa, Wako-Shi, Saitama 351-0198, Japan. [12]University of Alabama, NASA/Marshall Space Flight Center, Huntsville, AL 35899, USA. [13]NASA/Goddard Space Flight Center, Code 661, Greenbelt, MD 20771, USA. [14]Institute of Space and Astronautical Science, 3-1-1 Yoshinodai, Sagamihara, Kanagawa 229-8510, Japan. [15]Russian Academy of Sciences, Special Astrophysical Observatory Nizhnij Arkhyz, Zelenchukskaya, Karachaevo-Cherkesia 369167, Russia. [16]NASDA, National Space Development Agency of Japan, WTC Building 2-4-1, Hamamatsu-cho Minato-ku, Tokyo 105-60, Japan.

*To whom correspondence should be addressed. E-mail: piro@ias.rm.cnr.it

tical spectroscopy (*26*). This system should then be in the host galaxy of the GRB, which has probably been identified in deep optical images (*27*).

The detection of the line, the measurement of the distance (D = 4.7 Gpc, assuming Hubble constant $H_0 = 75$ km s^{-1} Mpc^{-1} and deceleration parameter $q_0 = 0.5$), and the fact that the driving process is recombination allow us to derive a lower limit on the mass of the line-emitting medium. The number of iron atoms $N_{\rm Fe}$ needed to produce the observed photon line luminosity $L = 10^{52}L_{52} = 8 \times 10^{52}$ photons s^{-1} is $N_{\rm Fe} = L_{\rm L}t_{\rm rec}$, where each of the $N_{\rm Fe}$ iron atoms produces $t_{\rm rec}^{-1}$ line photons per second (hereafter, some quantities are expressed as $Y = Y_n \times 10^n$). The recombination time of iron (*2*) is $t_{\rm rec} = 30\, T_7^{1/2} n_{10}^{-1}$ s, where $T = 10^7 T_7$ K and $n = 10^{10} n_{10}$ cm^{-3} are the temperature and density of the electrons, respectively. The temperature is constrained from the width of the recombination edge to be $k_{\rm B}T > 1$ keV, therefore implying $t_{\rm rec} > 30\, n_{10}^{-1}$ s. The total mass of material in the line region can be written

$$M = M_{\rm Fe}/(X_{\rm Fe}\, 1.8 \times 10^{-3}) > 7 X_{\rm Fe}^{-1} L_{52} n_{10}^{-1} M_\odot \quad (1)$$

Here, $X_{\rm Fe}$ is the iron abundance relative to the sun, where the iron is a fraction 1.8×10^{-3} of the total mass. The requirement that the ionization parameter ξ must be high enough to keep the Fe in a H-like state [$\xi = 4\pi D^2 F_X / nR^2 > 10^4$ (*25*)] allows us to estimate $n_{10} <$ 15, where we have used the flux observed by Chandra of $F_X = 2.3 \times 10^{-12}$ erg cm^{-2} s^{-1} and assumed that the distance of the gas from the GRB is $R > 2 \times 10^{15}$ cm. The latter condition derives from the presence of the line 1.5 days after the GRB, which, in the cosmological rest frame of the burst, is shorter than observed by a factor of $(1 + z)^{-1}$. Using this limit on the density and the observed line luminosity allows us to set a lower limit on the mass,

$$M \gtrsim 5 X_{\rm Fe}^{-1} M_\odot;\ M_{\rm Fe} \gtrsim 0.01 M_\odot \quad (2)$$

This large mass is not ejected during the GRB explosion, but in an earlier phase. This is the only possible condition under which the material would be moving at subrelativistic speed (as shown below) and be illuminated by GRB photons. The large mass of pre-ejected material excludes progenitor models based on double neutron star, black hole–neutron star, and black hole–white dwarf systems. These systems eject material long before they actually merge, and the progenitors of these GRBs travel far from their formation sites (and their ejecta) before producing a GRB (*1*). Conversely, massive progenitors—which evolve more rapidly—lead to a GRB in a mass-rich environment.

Additional information on the origin of the ejecta is derived from the line width ($\sigma_{\rm L}$ = 0.23 ± 0.07 keV, Fig. 1). Thermal broadening [$\Delta E/E = (k_{\rm B}T)^{1/2}$, where $k_{\rm B}T$ is expressed as $Am_{\rm p}c^2$; A is the atomic weight of iron, $m_{\rm p}$ is proton mass, and c is the speed of light] is negligible here, whereas Compton broadening would require a Thompson optical depth $\tau > 1$, which is excluded by (*3*). The line width is therefore kinematical, with velocity $v \approx 0.1c$. Normal winds from stars are not compatible with the parameters of the medium. In fact, the wind density is $n \approx 10^3\, \dot{M}_{-4} R_{16}^{-2} (v/0.1c)^{-1}$ cm^{-3}. Even for a high value of the mass loss rate $\dot{M}_{-4} = \dot{M}/(10^{-4} M_\odot\ {\rm year}^{-1}) = 1$, the density is orders of magnitude lower than that required to produce the observed line flux. Weth *et al.* (*9*) argued that high-density clouds could be produced from a low-density and low-velocity wind, but it remains to be assessed how those clouds could be accelerated to high velocities. Alternatively, nearly all the formation scenarios of GRB progenitors involve substantial mass loss when the system is in a common-envelope phase, a process that is likely to form a disk (*28*). Interaction of the expanding shell of the GRB with the disk could produce a shock-heated gas with density and velocity of the same order of magnitude as needed here (*10*). The emission from this region can be represented by pure thermal plasma (i.e., in thermal and collisional ionization equilibrium), but in this case emission from a recombination edge is negligible (*10*). To effectively ionize iron atoms, electrons should have a temperature comparable to the edge energy, therefore producing a feature too smeared to be detected. This may be circumvented if the electron population of the shock-heated plasma does not reach complete equilibrium, but the conditions under which this happens have yet to be studied. The simplest explanation of our results is a mass ejection by the progenitor with the same velocity implied by the observed line width. The ejection should have then occurred $\approx R/v$ (i.e., a few months) before the GRB.

The distribution of ejecta and the GRB emission are not highly anisotropic. Let $\Delta\Omega$ be the solid angle of the medium illuminated by the GRB and ΔR its size. The mass contained in the line-emitting volume is $M = \Delta\Omega R^2 \Delta R n m_{\rm p}$. Substituting the limit of the mass derived in the left side of Eq. 1 and the limits $\tau = \Delta R n \sigma_{\rm T} < 1$ and $\xi > 10^4$ (where $\sigma_{\rm T}$ is the Thomson cross section for scattering), we derive

$$\Delta\Omega/4\pi \gtrsim 60 X_{\rm Fe}^{-1} > 0.1 \quad (3)$$

where the lower limit corresponds to the extreme case of ejecta of pure iron. The GRB emission and the distribution of the medium around it therefore cannot deviate substantially from isotropy. The lower limit we have derived on the beaming factor (*29*) is marginally compatible with the estimate of (*20*). We note, however, that our results refer to the emission inside the line-emitting region, whereas the measurements mentioned above are based on the appearance of a break in the light curve 2 to 5 days after the GRB (i.e., when the fireball has overcome the line re-

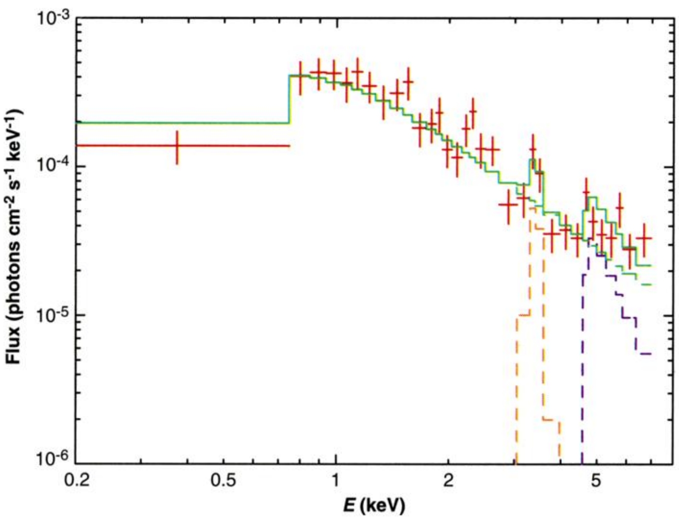

Fig. 2. The x-ray afterglow spectrum of GRB991216 obtained with the Chandra ACIS-S (0th order). The energy resolution of ACIS-S is 0.1 keV (full width at half-maximum) at 4 keV, and the background is negligible on the whole energy range. The better response at high energies compared to the gratings allows us to single out the presence of a further emission feature. Fitting a model (continuous green line) composed by an emission edge (blue dashed line) plus a power law (green dashed line) plus an emission line (orange dashed line) provides a satisfactory fit (χ_ν^2 = 0.95, degrees of freedom ν = 26) to the data (red crosses). The addition of the edge improves the fit by $\Delta\chi^2/\chi_\nu^2$ = 16.3, which corresponds to a confidence level of 99.5% (F test). Best-fit parameters of the edge are E = 4.4 ± 0.5 keV, $I_{\rm edge}$ = 3.8 (±2.0) × 10^{-5} photons cm^{-2} s^{-1}, and width $\sigma_{\rm edge}$ > 1 keV. For the power law we derive F_X(2 to 10 keV) = 2.3 × 10^{-12} cm^{-2} s^{-1}, photon index Γ = 2.2 ± 0.2, absorption column density $N_{\rm H}$ = 0.35 (±0.15) × 10^{22} cm^{-2}, consistent with the absorption in our galaxy ($N_{\rm HG}$ = 0.21 × 10^{22} cm^{-2}). Line parameters are consistent with those derived from the grating. Moreover, the edge is consistent with the grating data, as shown by the dotted line in the inset of Fig. 1.

gion). It is then possible that the initial GRB emission is isotropic and is then collimated by the interaction with a funnel-like medium. This limit on anisotropy allows the determination of the total, isotropic, electromagnetic energy produced by a GRB, which for GRB991216 is $E > 7.2 \times 10^{52}$ erg s^{-1} = $0.04 M_{\odot} c^2$. Another important implication of the previous limit is on the iron abundance of the medium, which must be much higher than solar ($X_{Fe} > 60$). This high value of the iron abundance indicates that the ejecta were—at some stage of the progenitor evolution—produced by a supernova explosion (*30, 31*).

In conclusion, the most straightforward scenario that emerges from all the pieces of evidence we have gathered is the following. A massive progenitor—like a hypernova or a collapsar (*32, 33*)—ejects, shortly before the GRB, a substantial fraction of its mass. This event is similar to a supernova explosion, as in the case of the SupraNova model (*34*).

References and Notes

1. C. L. Fryer, S. E. Woosley, D. H. Hartman, *Astrophys. J.* **526**, 152 (1999).
2. P. Mészáros, M. J. Rees, *Mon. Not. R. Astron. Soc.* **299**, L10 (1998).
3. M. Boettcher, C. D. D. Dermer, A. W. Crider, E. D. Liang, *Astron. Astrophys.* **343**, 111 (1999).
4. R. Perna, A. Loeb, *Astrophys. J.* **501**, 467 (1998).
5. R. A. M. J. Wijers, T. J. Galama, *Astrophys. J.* **523**, 177 (1999).
6. R. Sari, T. Piran, R. Narayan, *Astrophys. J.* **497**, L17 (1998).
7. D. Lazzati, G. Ghisellini, S. Campana, *Mon. Not. R. Astron. Soc.* **304**, L31 (1999).
8. M. Vietri, G. C. Perola, L. Piro, L. Stella, *Mon. Not. R. Astron. Soc.* **308**, L29 (2000).
9. C. Weth, P. Meszaros, T. Kallman, M. Rees, *Astrophys. J.* **534**, 581 (2000).
10. M. Boettcher, C. L. Fryer, in preparation (available at http://xxx.lanl.gov/abs/astro-ph/0006076).
11. L. Piro *et al.*, *Astrophys. J.* **514**, L73 (1999).
12. A. Yoshida *et al.*, *Astron. Astrophys.* **138**, 433 (1999).
13. Y. Daisuke *et al.*, *Publ. Astron. Soc. Japan* **52**, 509 (2000).
14. S. R. Kulkarni *et al.*, *Proc. 5th Huntsville GRB Symposium*, in press (available at http://xxx.lanl.gov/abs/astro-ph/0002168).
15. M. C. Weisskopf, S. O'Dell, L. P. van Speybroeck, *Proceedings of Multilayer and Grazing Incidence X-Ray/EUV Optics III*, R. B. Hoover, A. B. Walker, Eds. (SPIE Press, Bellingham, WA, 1996), p. 2.
16. R. M. Kippen, R. D. Preece, T. Giblin, *GCN Circular 463* (2000); *GCN Circular 504* (2000).
17. T. Takeshima, C. Markwardt, F. Marshall, T. Giblin, R. M. Kippen, *GCN Circular 478* (2000).
18. K. Hurley *et al.*, *GCN Circular 484* (2000); *GCN Circular 505* (2000).
19. L. Piro *et al.*, *GCN Circular 500* (2000).
20. J. P. Halpern *et al.*, *Astrophys. J.*, in press (available at http://xxx.lanl.gov/abs/astro-ph/0006206).
21. D. A. Frail *et al.*, *Astrophys. J.*, in press (available at http://xxx.lanl.gov/abs/astro-ph/0003138).
22. L. Piro, *Proceedings of UV and X-ray Spectroscopy of Laboratory and Astrophysical Plasmas*, E. Silver, S. Kahn, Eds. (Cambridge Univ. Press, Cambridge, 1993), p. 448.
23. F. Paerels, E. Kuulkers, J. Heise, J. in 't Zand, D. Liedahl, *Astrophys. J.* **535**, L25 (2000).
24. L. Amati *et al.*, *Science* **290**, 953 (2000).
25. T. R. Kallmann, R. McCray, *Astrophys. J. Suppl. Ser.* **50**, 263 (1983).
26. P. M. Vreeswijk *et al.*, *GCN Circular 496* (2000).
27. S. G. Djorgovski *et al.*, *GCN Circular 510* (2000).
28. The common-envelope phase happens when the hydrogen envelope of the secondary star expands, engulfing the compact primary (neutron star or black hole). Friction and tidal forces cause the compact object to spiral in the giant's core, ejecting the hydrogen envelope preferentially along the orbital plane, forming a disk [E. Sandquist, R. E. Taam, X. Chen, P. Bodenheimer, A. Burkert, *Astrophys. J.* **500**, 909 (1998)].
29. The beaming factor $\Delta\Omega/4\pi$ is the fraction of sky over which GRB photons are emitted. It is equal to 1 if the emission is isotropical and $\approx \theta^2/4$ in the case of a jet with opening angle θ.
30. S. E. Woosley, T. A. Weaver, *Astrophys. J. Suppl. Ser.* **101**, 181 (1995).
31. P. Bouchet *et al.*, *Astron. Astrophys.* **245**, 490 (1991).
32. B. Paczynski, *Astrophys. J.* **494**, L45 (1998).
33. S. E. Woosley, *Astrophys. J.* **405**, 273 (1993).
34. M. Vietri, L. Stella, *Astrophys. J.* **507**, L45 (1998).
35. See Chandra calibration reports (http://asc.harvard.edu/cal).

36. We thank the Chandra team for support, in particular F. Nicastro and A. Fruscione for help in data reduction; M. Boettcher for critical suggestions; G. Ricker for useful discussions on the observational strategy; and L. A. Antonelli for comments. Supported by NASA contract NAS8-39073 to the Chandra X-ray Center (M.G.).

5 September 2000; accepted 10 October 2000

Mode-Specific Energy Disposal in the Four-Atom Reaction $OH + D_2 \rightarrow HOD + D$

Brian R. Strazisar, Cheng Lin, H. Floyd Davis*

Experiments, employing crossed molecular beams, with vibrational state resolution have been performed on the simplest four-atom reaction, $OH + D_2 \rightarrow HOD + D$. In good agreement with the most recent quantum scattering predictions, mode-specific reaction dynamics is observed, with vibration in the newly formed oxygen-deuterium bond preferentially excited to $v = 2$. This demonstrates that quantum theoretical calculations, which in the past decade have achieved remarkable accuracy for three-atom reactions involving three dimensions, have progressed to the point where it is now possible to accurately predict energy disposal in four-atom reactions involving six dimensions.

A central goal in the study of chemical reaction dynamics is to understand the details of how bonds are broken and formed during a reaction (*1*). The potential energy surface (PES), which describes how the potential energy of the system depends on the relative position of the atoms, may be derived using ab initio or density functional theory (*2*). Classical, quasi-classical, or quantum scattering calculations may be carried out using the PES to understand which collision geometries and forms of reactant energy (such as translational or vibrational) facilitate passage through the transition state region to the chemical products (*3, 4*). Scattering calculations can also predict product quantum state distributions as a function of scattering angle (*3, 4*).

The accuracy of theoretical calculations may be tested by comparing predicted product quantum state and angular distributions to those measured experimentally (*3–5*). To date, studies of three-atom systems (A + BC $\rightarrow$ AB + C), using crossed molecular beams, have provided the most detailed insight into the mechanisms and energy disposal in chemical reactions (*5–11*). Recent studies of the $H + D_2 \rightarrow HD + D$ (*6, 7*) and $O + H_2 \rightarrow OH + H$ (*11*) reactions have employed the high-resolution H atom Rydberg tagging method (*12*) to determine the vibrational and rotational energy distributions of the diatomic products as a function of scattering angle.

A more recent challenge to both theoreticians and experimentalists has been the study of four-atom reactions (AB + CD $\rightarrow$ ABC + D or ABC + D $\rightarrow$ AB + CD). In three-atom systems, internal excitation is limited to two rotational and one vibrational degree of freedom in the diatomic reactant and product. In four-atom reactions, the triatomic reactant or product (if nonlinear) has three vibrational degrees of freedom, some involving motion of the newly broken or formed bond. When a triatomic molecule is produced in a four-atom reaction, it becomes possible to ask not only how much energy is deposited into product vibration, but also how energy is distributed among the vibrational modes.

Mode-specific behavior is an important feature of reaction dynamics involving four-atom systems. Excitation of the OH stretching mode of H_2O greatly enhances the rate of the $H + H_2O \rightarrow OH + H_2$ reaction, whereas excitation of the H_2O bending mode has no effect (*13, 14*). In the H + HOD reaction, selective excitation of either the OH or OD stretching overtone (*13*) or fundamental (*15*) in HOD can dictate which bond is reactive. From the principle of microscopic reversibility, preferential vibrational excitation of the new bond in the reverse reaction might be

Department of Chemistry and Chemical Biology, Cornell University, Ithaca, NY 14850, USA.

*To whom correspondence should be addressed. E-mail: hfd1@cornell.edu